# CHAPTER 4

**To model the inactivation kinetics of enzyme (pectin methylesterase) and microbe (*Escherichia coli)* in orange juice during atmospheric cold plasma processing**

# To model the inactivation kinetics of enzyme (pectin methylesterase) and microbe (*Escherichia coli)* in orange juice during atmospheric cold plasma processing

## 4.1 Introduction

Pectin methylesterase (PME) is an enzyme naturally present in oranges that significantly influences the texture and stability of the orange juice. It is responsible for the quality deterioration of juice during processing and storage (Lacroix et al., 2005; Arya et al., 2023). Several studies have demonstrated that cold plasma (CP) can significantly inactivate the various endogenous enzymes in fruit and vegetable juice (Xu et al., 2017; Andreou et al., 2023; Sauza et al., 2023). The *Escherichia coli* (*E. coli*), a commonly studied bacterium in food safety, can cause foodborne illnesses (Pokhrel et al., 2017). Maintaining microbiological safety in beverage and juice production is a major concern, as juices are often consumed raw or minimally processed, which increases the risk of contamination. Several conventional heat-based and non-thermal technologies have also been employed to decontaminate or inactivate the various microbes in foods through processing (Lee et al., 2009; Hosseini et al., 2020; Van Impe et al., 2018; Liao et al., 2018; Pokhrel et al., 2017). Namouras studies reported that non-thermal CP has a potential application for the inactivation of *E. coli* in food products (Santos et al., 2018; Sauza et al., 2023; Hosseini et al., 2020; Mošovská et al., 2023). However, inactivation kinetics modelling using mathematical equations is crucial for food safety, quality retention, and process optimisation. Therefore, this study focused on the inactivation kinetics modelling of PME enzyme and *E. coli* in orange (cv. Wakro) juice during atmospheric cold plasma (ACP).

## 4.2 Materials and Methods

### 4.2.1 Raw materials and chemicals

The raw materials, oranges (cv. Wakro) of Northeast India origin cultivated across Arunachal Pradesh, were procured from the local vendor in the Tezpur area, Assam, India. Pectin, Luria-Bertani Broth agar (LBA), NaCl, and NaOH were purchased from HiMedia Laboratories Pvt. Ltd., India, and Merck Specialities Pvt. Ltd., India.

### 4.2.2 Juice preparation

The 'Wakro' cultivar of oranges was procured from the local market of the Tezpur area, Assam. The oranges were cleaned and rinsed, split into two pieces using a knife, and then manually squeezed by a stainless-steel Dynore juicer. Further, the juice was strained through two layers of fine muslin cloth. The Brix-acid ratio of squeezed filtered juice was standardized at constant (ºBrix/acid ≈ 30) by maintaining total soluble solids (TSS) and titratable acidity (TA) at 12.2 ± 0.10 ºBrix and 0.41 ± 0.02% (Kumar et al., 2024).

### 4.2.3 Experimental design

A full factorial design was used to plan the experimental runs with voltage (16, 20, and 24 kV) and treatment time (0.5, 1, 1.5. 2, 2.5, and 3 min). The dependent parameters were the residual activity (RA) of the PME enzyme and log CFU/mL of *E. coli*. In this study, the juice sample depth was constant at 4.6 mm (as obtained from objective 1). The gap between electrodes was fixed at 15 mm during ACP treatment. The detailed experimental plan for the kinetic study of PME enzyme and *E. coli* inactivation is presented in **Fig. 4.1.**

### 4.2.4 Atmospheric cold plasma treatment

The schematic diagram of the ACP system and treatment process is shown in **Fig. 4.2**. The ACP device consists of dielectric barrier plates, a treatment chamber, a voltage regulator, gas inlet and outlet pipes, and a glass cover. In this study, a known amount (23 mL, i.e., 4.6 mm depth) of juice was poured onto a petri dish (diameter: 80 mm) and placed in a treatment chamber for the ACP treatment with different voltage and treatment time combinations. After treatment, the juice was immediately taken out to analyze PME activity and the survival population of *E. coli*.

### 4.2.5 Enzyme (pectin methylesterase) activity

PME activity in orange (cv. Wakro) juice was determined using the titration method according to the assay described by Basak and Ramaswamy (1996) and the detailed procedure is mentioned in **Section 3.2.6** of **Chapter 3**.

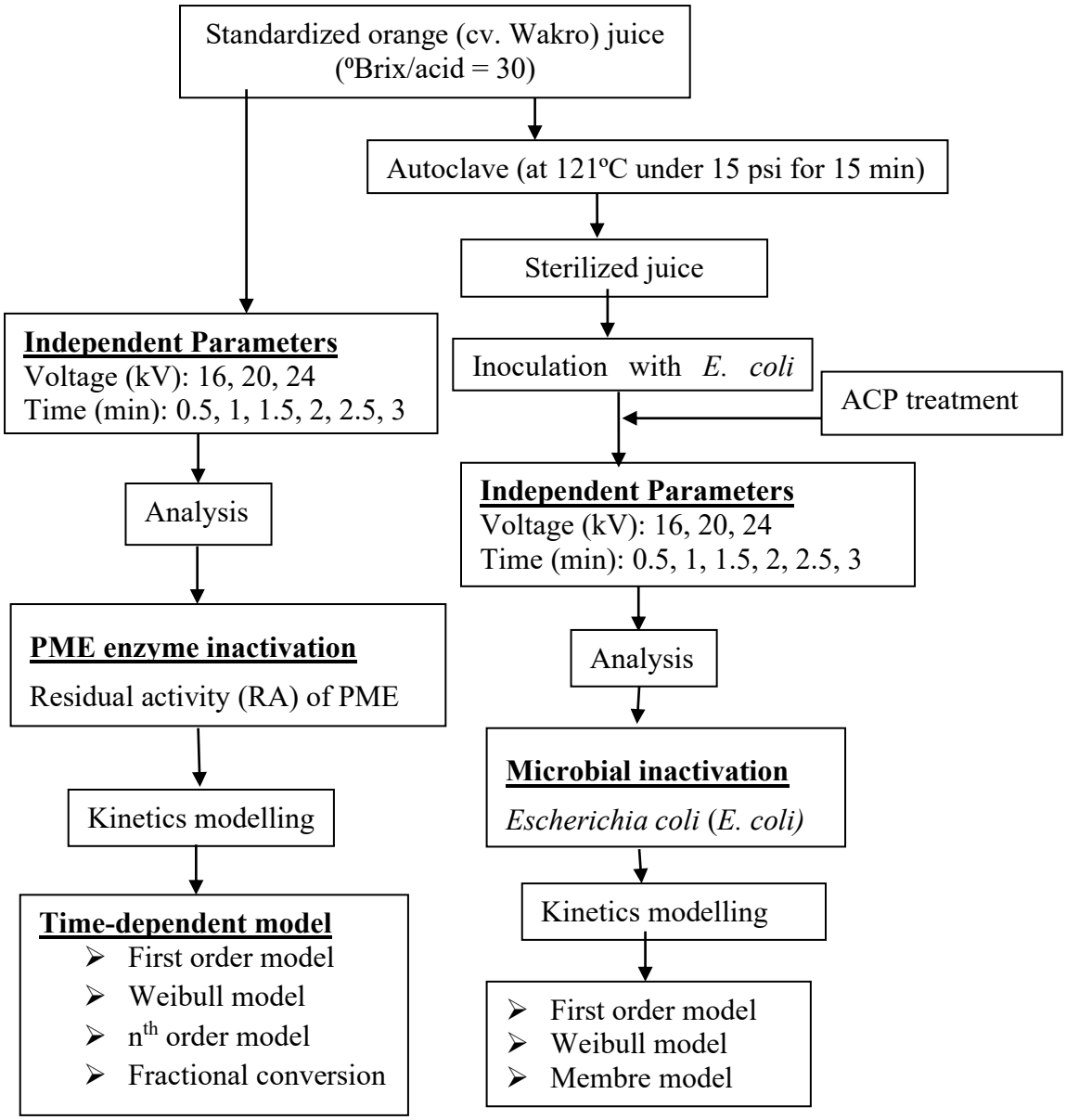


**Fig. 4.1** Detailed work plan for objective 2.

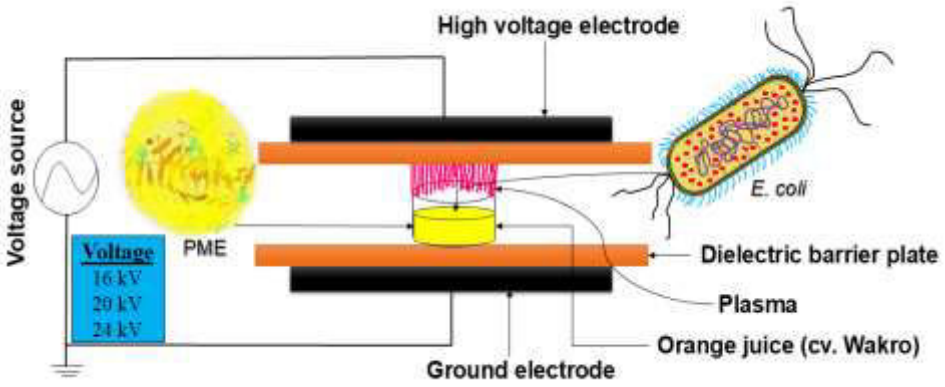


**Fig. 4.2** Schematic diagram of atmospheric cold plasma (ACP) treatment on enzyme (pectin methylesterase) and microbe (*Escherichia coli*) in orange (cv. Wakro) juice.

### 4.2.6 Microbial (*Escherichia coli)* analysis

The microbial load in untreated and ACP-treated juice samples was measured using the standard FDA's Bacteriological Analytical Manual (BAM) methods (2001). A pour plate method with serial dilutions (up to $10^{-5}$) was employed to determine the log CFU/mL of *E. coli* (MTCC 40) in orange (cv. Wakro) juice before and after ACP treatment. Saline water was prepared by adding 0.85% NaCl (w/v). A 15–20 mL LBA solution was poured into the sterile petri plates and solidified for 30 min at room temperature. After plating the microbial cultures, the plates were incubated at 37 ºC for 24 h. The colonies in plates were enumerated manually and expressed as CFU/mL, as shown in **Eq. 4.1**.

$$CFU/mL = \frac{Number\ of\ colonies \times total\ dilution\ factor}{Volume\ of\ culture\ plated\ in\ mL} \quad (4.1)$$

$$\text{Log}\, reduction = log_{10}(N_0) - log_{10}(N_t) \quad (4.2)$$

Where, '$N_0$' is the initial viable counts of *E. coli* before treatment, '$N_t$' is the viable count of *E. coli* after treatment at a time 't.'

### 4.2.7 Enzyme inactivation kinetics models

The first-order model is commonly used for characterizing the inactivation kinetics of various enzymes in fruits and vegetable products during processing (Ludikhuyze et al., 1999; Pankaj et al., 2013). The first-order model was expressed in **Eq. 4.3.**

$$\frac{A_t}{A_0} = exp(-k_p t) \quad (4.3)$$

Where, $k_p$ is the inactivation rate constant, $min^{-1}$.

The two-parameter Weibull distribution model was fitted to evaluate kinetic behavior**,** as shown in **Eq. 4.4** (Pankaj et al., 2013).

$$\frac{A_t}{A_0} = \exp\left[-\left(\frac{t}{\delta}\right)^{\beta}\right] \quad (4.4)$$

Where, $\beta$ is the shape factor (dimensionless), and $\delta$ is the scale factor (min). The $\beta$ indicate the survival curve's convexity (shoulder-forming) or concavity (tailing-forming). $\beta < 1$, denotes upward concavity and $\beta > 1$ represents downward concavity. $\beta = 1$, it would correspond to the first-order or linear kinetic model.

The $n^{th}$ order model for $n \neq 1$ was expressed in **Eq. 4.5** (Weemaes et al., 1998).

$$\frac{A_t}{A_0} = \left\{A_0{}^{(1-n)} + (n-1)k_s t\right\}^{\frac{1}{(1-n)}} \quad (4.5)$$

Where 'n' represents the order of the reaction in the n$^{th}$-order model.

The fractional conversion model is tested for a highly heat-resistant or plasma-resistant enzyme fraction that remains after prolonged treatment (Shalini et al., 2008). This non-linear kinetic model was expressed in **Eq. 4.6** (Rizvi and Tong, 1997).

$$\frac{A_t}{A_0} = A_r + \{(A_0 - A_r)\exp(-k_f t)\} \quad (4.6)$$

Where, $A_r$ is the fractional resistant, $k_f$ is the inactivation rate constant.

### 4.2.8 Microbe (*Escherichia coli)* inactivation kinetics models

The log-linear model assumes that microbial inactivation follows first-order kinetics. This equation suggests that the logarithmic reduction in microbial population over time follows a straight line, with the slope of the line being the inactivation rate constant, $k_m$. The simplified log-linear model for microbial (*E. coli*) inactivation was expressed in **Eq. 4.7**.

$$log\left(\frac{N_t}{N_0}\right) = -\frac{k_m t}{\ln(10)} \quad (4.7)$$

The Weibull model with two parameters is widely used for the kinetics of *E. coli* inactivation, as shown in **Eq. 4.8** (Liao et al., 2018).

$$log\left(\frac{N_t}{N_0}\right) = -\frac{1}{2.303}\left(\frac{t}{\delta}\right)^{\beta} \quad (4.8)$$

The Membré model is a mathematical approach developed by Membré et al. (1997) to characterize various microorganisms' thermal and non-thermal inactivation kinetics in foods. This model is also named a convex model due to the convex shape of the survival curve. The convex model was tested for the inactivation kinetics of *E. coli*, as shown in **Eq. 4.9**.

$$logN_t = (1 + logN_0) - \exp(k_c t) \quad (4.9)$$

Where, $k_c$ is the inactivation rate constant, min$^{-1}$.

### 4.2.9 Goodness-of-fit parameters

The statistical parameters, the coefficient of determination ($R^2$), and root mean square error (RMSE) were considered to assess the goodness-of-fit of the proposed regression models in the kinetic study **(**Kumar and Srivastava, 2024). The equations of $R^2$ and RMSE are shown in **Eq. 4.10** and **4.11**. The $R^2$ determines how well the regression model fits the observed data. The $R^2$ is a valid statistical parameter for examining the potency of any mathematical model. The ranges of $R^2$ values lie between 0 and 1; $R^2$ values close to one indicate a perfect fit.

$$R^2 = 1 - \frac{\sum_{i=1}^{n}(Y_i - Y_p)^2}{\sum_{i=1}^{n}(Y_i - Y_a)^2} \tag{4.10}$$

The RMSE calculates the magnitude of errors produced by a regression model. A lower value of RMSE indicates the model is well-fit, which means the observed values are closer to the predicted values.

$$RMSE = \sqrt{\frac{1}{n}\sum_{i=1}^{n}\left(Y_i - Y_p\right)^2} \tag{4.11}$$

Where 'n' is the number of observations, '$Y_i$' and '$Y_p$' are observed and predicted values, and '$Y_a$' is the average observed value, respectively.

### 4.2.10 Model assessment and validation

The accuracy factor ($A_f$) and bias factor ($B_f$) have been used for model validation and performance evaluation, which was proposed by Ross (1996). **Eq. 4.12** and **4.13** were used with a set of observed data for this purpose (Vega et al., 2016).

$$A_f = 10^{\sum_{i=1}^{n}\left|\log\left(Y_p/Y_i\right)\right|/n} \tag{4.12}$$

$$B_f = 10^{\sum_{i=1}^{n}\{\log\left(Y_p/Y_i\right)\}/n} \tag{4.13}$$

Where 'n' is the total number of observations. The $A_f$ represents how well the prediction ties the observations (close to 1 indicates little deviations). The $B_f$ shows whether the observed data lie above or below the prediction line. The $B_f$ >1 represents over prediction, $B_f$ < 1 indicates under-prediction, and $B_f$ = 1 implies exact prediction (Pipliya et al., 2022).

### 4.2.11 Model Selection Criteria

#### 4.2.11.1 Akaike information criterion

It is essential that reasonably, sometimes multiple models fit equally well in a particular given set of data, and those data sets do not support selecting one model (Kumar and Srivastava, 2024). The Parsimony principle states that, out of the several competing models, the one with the lowest number of model parameters should be considered (Vega et al., 2016). However, in addition to this, other parameters should be considered to segregate the competing models (Kumar and Srivastava, 2024). Akaike information criterion (AIC) ranks, discriminates, and selects the best model among multiple competing models, as shown in **Eq. 4.14** (Serment-Moreno et al., 2015).

$$AIC = -2l + 2m;\ l = -\frac{n}{2}\ln(\hat{\sigma}^2) \tag{4.14}$$

Where 'm' is the number of model parameters, '$\hat{\sigma}^2$' is the variance, and 'l' is the maximum log-likelihood estimate.

#### 4.2.11.2 Akaike increment

The smallest AIC makes ranking the model for assessing the specific data set simple. Based on the AIC values, the model with the lowest AIC value will receive a value of 0, and the subsequent model that comes after receiving a value greater than 0; this is known as the Akaike increment ($\Delta_i$) (**Eq. 4.15**) (Akaike, 1998).

$$\Delta_i = AIC_i - AIC_{min} \tag{4.15}$$

Where, $AIC_{min}$corresponds to the best candidate model with the smallest AIC value. However, $\Delta_i$ values are straightforward and allow for easy comparison, interpretation, and ranking of competing models (Kumar and Srivastava, 2024). The fitted models are evaluated and chosen according to the following criteria: models with $\Delta_i \leq 2$ are considered to have strong support; those with $2 \leq \Delta_i \leq 10$ are regarded as having considerably less support, and models with $\Delta_i > 10$ are deemed to have no support across all model selections (Burnham and Anderson, 2001).

### 4.2.12 Statistical analysis

The results of the experiments were expressed as mean ± standard deviation (SD). Inactivation kinetics modelling was done using MATLAB R2015a software. Statistical parameters $R^2$ and RMSE were obtained from MATLAB. Other statistical parameters like $A_f$, $B_f$, AIC, and $\Delta_i$ were calculated using Microsoft Excel 2021.

## 4.3 Results and Discussion

### 4.3.1 Effect of ACP treatment on PME inactivation

The PME activity in orange (cv. Wakro) juice was significantly inactivated during ACP treatment (voltage: 16–24 kV, treatment time: 0.5–3 min), as can be seen in **Fig. 4.3**. The RA of PME in juice decreased from 100 ± 0.00% to 14.67 ± 1.89% for 3 min at voltage 24 kV, indicating a maximum 85.33% inactivation. The 24 kV voltage enhanced the plasma intensity and the generation of reactive species during the 3-min treatment. As a result, the oxidative damage and mechanical disruption from plasma contributed to a significant PME inactivation. On the other hand, PME inactivation was achieved by 58.55% and 70.67% for 3 min treatment duration at voltages of 16 kV and 20 kV, respectively. The study's results revealed that the PME inactivation was significantly influenced by voltage and plasma exposure time. It was observed that RA of PME decreased with increasing the treatment time at all voltages (**Fig. 4.3**). A study reported that the jet source CP with helium gas treatment (duration: 2–30 min, voltage: 4–7 kV) inactivated 55–80% PME enzyme in orange juice (Andreou et al., 2023). Xu et al. (2017) and Kumar et al. (2023) reported that enzyme inactivation in juice is also impacted by juice volume or depth in petri plates, the used working gas and its composition, the initial activity of enzymes, and the nature of fruits, and varieties, respectively. The mechanism involved in enzyme inactivation could be attributed to the interaction of plasma-generated reactive species with the enzyme structure. The consequence of this interaction leads to protein denaturation, thereby reducing enzyme functionality (Pankaj et al., 2018).

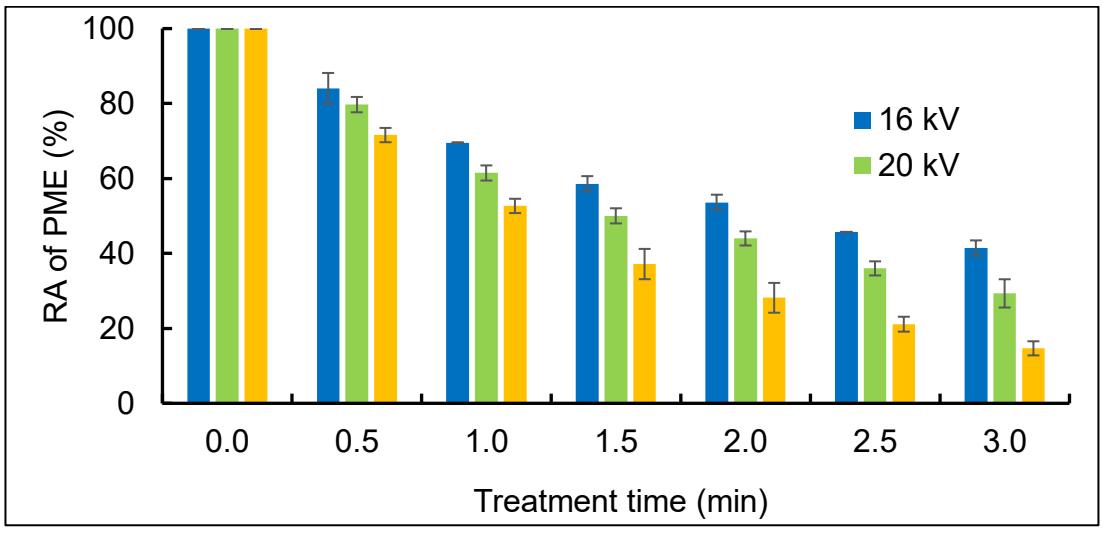


**Fig. 4.3** Effect of atmospheric cold plasma (ACP) on RA of PME.

### 4.3.2 Inactivation kinetics modelling of PME enzyme

As shown in **Fig. 4.4**, the curves illustrating the RA of PME decreased in juice during ACP treatment. An accurate kinetics modelling is crucial to understanding the behavior of PME activity reduction in juice by ACP. Therefore, the following suggested models were fitted for characterizing the kinetics behavior of PME.

**Table 4.1** Model constant and goodness of fit parameters for PME.

| Model | Parameters | PME | | |
|---|---|---|---|---|
| | | **16 kV** | **20 kV** | **24 kV** |
| First-order | $k_p$ ($min^{-1}$) | 0.3205 ± 0.04 | 0.4304 ± 0.04 | 0.6386 ± 0.03 |
| | $R^2$ | 0.9879 | 0.9923 | 0.9991 |
| | RMSE | 0.0234 | 0.0221 | 0.0092 |
| Weibull | β | 0.8548 ± 0.15 | 0.8847 ± 0.14 | 0.9552 ± 0.05 |
| | δ (min) | 3.3760 ± 0.43 | 2.3960 ± 0.21 | 1.5640 ± 0.05 |
| | $R^2$ | 0.9964 | 0.9972 | 0.9997 |
| | RMSE | 0.0140 | 0.0146 | 0.0061 |
| $n^{th}$ order | $k_s$ ($min^{-1}$) | 0.4095 ± 0.12 | 0.5163 ± 0.15 | 0.6789 ± 0.07 |
| | $A_0$ | 1.0040 ± 0.05 | 1.0030 ± 0.05 | 1.0000 ± 0.02 |
| | n | 1.6910 ± 0.75 | 1.4070 ± 0.58 | 1.1060 ± 0.14 |
| | $R^2$ | 0.9979 | 0.9978 | 0.9998 |
| | RMSE | 0.0120 | 0.0144 | 0.0058 |
| Fractional conversion | $k_f$ ($min^{-1}$) | 0.5269 ± 0.22 | 0.5819 ± 0.24 | 0.6953 ± 0.08 |
| | $A_0$ | 1.0030 ± 0.04 | 1.0010 ± 0.06 | 0.9998 ± 0.02 |
| | $A_r$ | 0.2630 ± 0.15 | 0.1568 ± 0.17 | 0.0413 ± 0.04 |
| | $R^2$ | 0.9981 | 0.9976 | 0.9998 |
| | RMSE | 0.0114 | 0.0150 | 0.0054 |

#### 4.3.2.1 First-order model

The first-order kinetics modelling for RA of PME at various voltages (16–24 kV) against time (0.5–3 min) is shown in **Fig. 4.4a**. In this model, the k value rose proportionally from 0.3205 to 0.6386 $min^{-1}$, increasing the voltage from 16–24 kV, indicating that voltage affected the PME activity in juice (**Table 4.1**) (**Fig. 4.4a**). A greater k ($min^{-1}$) was observed at high CP voltage (24 kV), as shown in **Fig. 4.4a** and **Table 4.1**. Pankaj et al. (2013), Chutia et al. (2019), Pipliya et al. (2022), and Dong et al. (2021) also observed a similar trend of inactivation rate constant, k concern with the CP voltage. The model's performance in terms of fit was adequate ($R^2$ = 0.9879–0.9991). In contrast, RMSE values were not desirable because they were correspondingly more significant than the Weibull, $n^{th}$-order, and fractional conversion models (**Table 4.1**). The previous studies reported that the first-order model is quite simple for explaining the enzyme inactivation kinetics after ACP treatment (Pankaj et al., 2013; Dong et al., 2021; Pipliya et al., 2022). This could be

attributed to the enzyme's complex structure and the varying methods by which different plasma reactive species break down the enzyme structure or individual bonds (Dong et al., 2021). However, the consequences suggest that the first-order model is unsuitable to describe the PME inactivation kinetics following ACP treatment.

#### 4.3.2.2 Weibull model

The Weibull model is usually used to describe the kinetics modelling of enzyme and microbial inactivation in diverse foods because of its flexibility and non-linearity character in the fitting curves (Dong et al., 2021; Pipliya et al., 2022). Therefore, the Weibull model was fitted into the experimental data to explain the kinetic behavior of RA of PME during ACP treatment. The scale factor (δ) and shape factor (β) of the Weibull model were obtained by fitting the data in **Eq. 4.4**. As shown in **Table 4.1**, δ values ranged from 3.3760 to1.5640 min, implying a relationship between high PME inactivation with increasing the applied voltage. The lower δ value of PME inactivation under ACP treatment conditions suggests a higher plasma stability in the juice sample. A high voltage may lead to rapid inactivation by producing more reactive species and free radicals, which impacts the δ value. The shape factor, $\beta < 1$, indicated a concave nature of the model curve for RA of PME (**Fig. 4.4b** and **Table 4.1**) and explained the tailing phenomena. Similar behavior of δ and β with CP voltage was reported by Kumar et al. (2023) and Pipliya et al. (2022) in kiwifruit juice and pineapple juice. As shown in **Table 4.1**, the $R^2$ values ranged from 0.9964–0.9997, indicating a strong fit with observed data for predicting the RA of PME. The low RMSE (0.0140–0.0061) was also more effective than the first order for predicting the PME inactivation.

#### 4.3.2.3 $n^{th}$ order model

The $n^{th}$-order model gives an insight into better understanding the mechanism in the non-linear kinetic behaviors associated with loss of enzyme activity in the food matrix during processing (Saxena et al., 2017). The parameters of the $n^{th}$-order model, like $k_s$, $A_o$, and n for the PME inactivation were calculated using **Eq. 4.5** and presented in **Table 4.1**. The inactivation kinetics curves of the $n^{th}$-order equation are shown in **Fig. 4.4c**. The inactivation rate constant, $k_s$ value for PME ranged from 0.4095 to 0.6789 $min^{-1}$ at 16–24 kV voltage levels. The RA of PME decreased with increasing the

voltage, indicating PME inactivation increased with the rise in CP voltage; this could be correlated with increasing the $k_s$value. The inactivation order (n) value varied from 1.6910 to 1.1060 at the applied voltage range of 16–24 kV, indicating the RA of PME decreased during ACP treatment (**Table 4.1).** The PME inactivation rate depends upon their structural stability and treatment time. Other studies also fitted the $n^{th}$-order model for characterizing the enzyme inactivation kinetics (Chakraborty et al., 2015; Saxena et al., 2017; Kumar et al., 2023). The coefficient of determination value for the $n^{th}$ order model was $R^2 > 0.98$ while RMSE < 0.013, suggesting a good fitting performance with the observed data (**Table 4.1**).

#### 4.3.2.4 Fractional conversion model

The fractional conversion model is specifically applicable for describing the inactivation kinetics of enzymes that show both resistant and liable characteristics while subjected to thermal and non-thermal treatment (Kumar and Srivastava, 2024). The values of model parameters such as $A_0$, $A_r$, and $k_f$ ($min^{-1}$) are presented in **Table 4.1**. The plasma-resistant fractions of PME were obtained from 0.2630 to 0.0413, indicating that $A_r$ decreased with increasing the applied voltage (**Table 4.1**). This suggests that the RA of PME required more treatment time at low voltage to achieve maximum PME inactivation. The $k_f$ values of the RA of PME were in the range of 0.5269–0.6953 $min^{-1}$, indicating that inactivation increased with the rise of voltage. The $R^2 > 0.99$ with low RMSE < 0.0055 values suggested the good fitting of the model (**Table 4.1**). However, it could not be confirmed with the goodness of fit parameter values for selecting the best model among the several competing models. Therefore, other statistical parameters ($A_f$, $B_f$, AIC, and $\Delta_i$) were assessed to select a best-fit model.

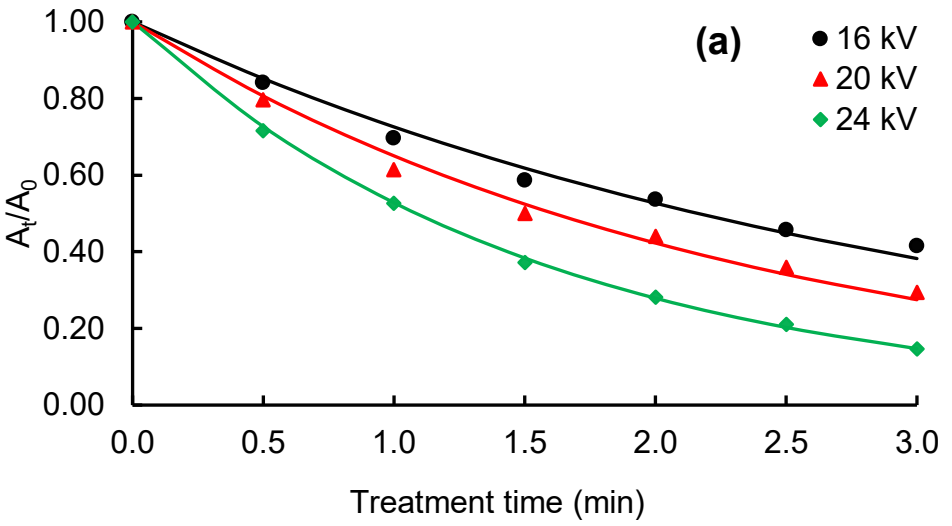
(a)
16 kV
20 kV
24 kV
$A_t/A_0$
1.00
0.80
0.60
0.40
0.20
0.00
0.0
0.5
1.0
1.5
2.0
2.5
3.0
Treatment time (min)

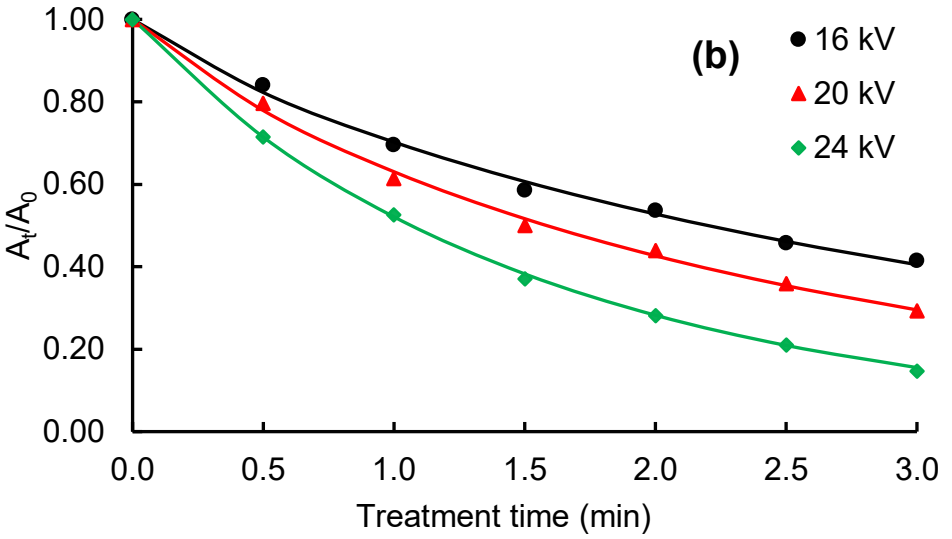
(b)
16 kV
20 kV
24 kV
$A_t/A_0$
1.00
0.80
0.60
0.40
0.20
0.00
0.0
0.5
1.0
1.5
2.0
2.5
3.0
Treatment time (min)

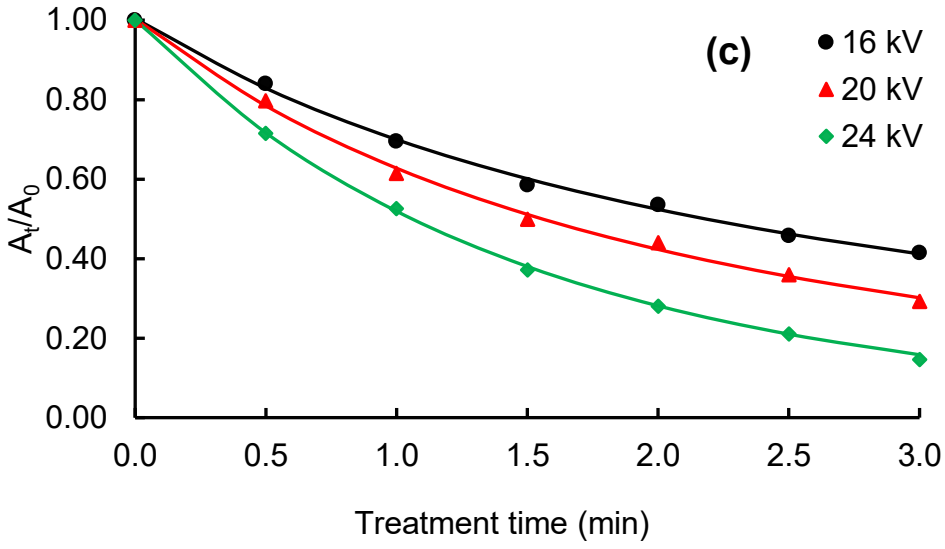
(c)
16 kV
20 kV
24 kV
$A_t/A_0$
1.00
0.80
0.60
0.40
0.20
0.00
0.0
0.5
1.0
1.5
2.0
2.5
3.0
Treatment time (min)

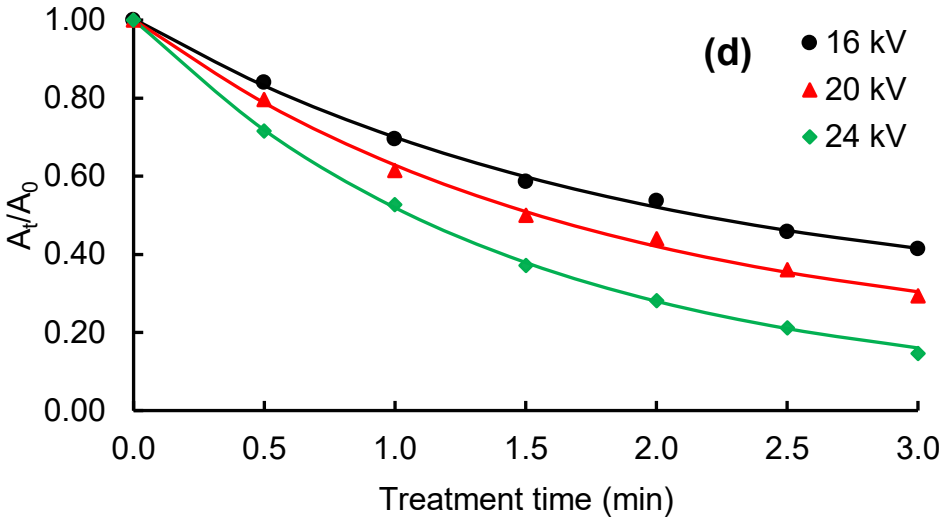


**Fig. 4.4** RA of PME kinetics at different voltages (16–24 kV) (a) First-order model, (b) Weibull model, (c) $n^{th}$-order model, (d) Fractional conversion model. Different color marks (▲, ♦, ●) and lines (—, —, —) in the graphs indicated the experimental and predicted values of the RA of PME.

### 4.3.3 Model validation and selection for PME inactivation

**Table 4.2** Model validation and selection for PME.

| Model | Parameters | PME | | |
|---|---|---|---|---|
| | | 16 kV | 20 kV | 24 kV |
| First order | $A_f$ | 1.0007 | 1.0005 | 1.0006 |
| | $B_f$ | 1.0007 | 1.0005 | 1.0006 |
| | AIC | -64.16 | -71.05 | -71.92 |
| | $\Delta_i$ | 0.00 | 0.00 | 0.00 |
| Weibull | $A_f$ | 1.0007 | 1.0005 | 1.0006 |
| | $B_f$ | 1.0052 | 1.0036 | 1.0041 |
| | AIC | -60.16 | -67.05 | -67.92 |
| | $\Delta_i$ | 4.00 | 4.00 | 4.00 |
| $n^{th}$ order | $A_f$ | 1.0007 | 1.0005 | 1.0006 |
| | $B_f$ | 1.0052 | 1.0036 | 1.0041 |
| | AIC | -62.16 | -69.05 | -69.92 |
| | $\Delta_i$ | 2.00 | 2.00 | 2.00 |
| Fractional conversion | $A_f$ | 1.0353 | 1.0007 | 1.0009 |
| | $B_f$ | 0.9659 | 1.0007 | 1.0009 |
| | AIC | -60.16 | -67.05 | -67.92 |
| | $\Delta_i$ | 4.00 | 4.00 | 4.00 |

#### 4.3.3.1 Performance of the models and its validation

The accuracy factors ($A_f$) in all the fitted models (first-order, Weibull, $n^{th}$-order, and fractional conversion) showed approximately 1, which indicates that observed data can be predicted with reasonable accuracy (**Table 4.2**). Vega et al., 2016 suggested that a model would be robust and reliable if the $B_f$ value is close to 1. The $B_f$ values in

all the fitted models exhibited close to 1 expect fractional conversion model at 16 kV (**Table 4.2**). $B_f < 1$ implies that the model fails to capture the complexity of the data, leading to underfitting. It was observed that the first-order, Weibull, and $n^{th}$-order models showed good precision with minimum error in the fitted curve. In this kinetic study, the fractional conversion model showed the same at 20 kV and 24 kV voltages. However, after examining the $A_f$ and $B_f$ factors, all the fitted models effectively predicted the experimental results with minimal error and maximum precision. The contradiction between goodness-of-fit parameters ($R^2$ and RMSE) and the validation indices ($A_f$ and $B_f$) arose because $R^2$ and RMSE promoted closer fits to the data. Still, they don't account for overfitting or model complexity (**Table 4.1** and **4.2**). In contrast, AIC and $\Delta_i$ are more robust in selecting models that generalize well, not just those that fit the data very closely. The low AIC and $\Delta_i$ values suggest the best-fitting model with easy comparison, interpretation, and ranking of competing models (Kumar and Srivastava et al., 2024). Therefore, AIC and $\Delta_i$ were employed to determine the best-fitting model from the tested competing models for predicting the RA of PME after ACP treatment.

#### 4.3.3.2 Model selection by the Akaike information criterion and Akaike increment

The AIC and $\Delta_i$ criteria were employed to pick the best model from the four aforementioned models. The computed values of AIC for Weibull and fractional conversion model were obtained more than the first-order and $n^{th}$-order models (**Table 4.2**). Nonetheless, Akaike increment also exhibited less substantial support ($\Delta_i$= 4) (**Table 4.2**). As a result, Weibull and fractional models cannot be considered for best-fit prediction. According to the Akaike increment thumb rule, these models showed substantially less support ($2 \leq \Delta_i \leq 10$) and should not be considered for overall model selection (Vega et al., 2016; Pipliya et al., 2022).

The AIC value of the first-order model was found to be the lowest, followed by the $n^{th}$-order model (**Table 4.2**). At all conditions, the calculated $\Delta_i$ value of the first-order model was found to be 0, which indicates that the model has significant support. However, looking into the goodness-of-fit parameters (RMSE: 0.0234–0.0092) were relatively higher than the other three models (**Table 4.1**). Consequently, it is challenging to select the best model. Kumar and Srivastava (2024) and Vega et al. (2016) reported that the first-order model should not be a primary choice. They

acknowledged that information criteria theory penalizes models more with more parameters. Finally, the $n^{th}$-order model estimated the second least AIC values with $\Delta_i = 2$ for the PME enzyme. This model was also supported by $A_f$ and $B_{f,}$ values close to the simulation line, and goodness-of-fit parameters ($R^2$ and RMSE) (**Table 4.1**). Thus, Akaike's criteria theory and other statistical parameters suggested that the $n^{th}$-order model should be the primary selection for predicting the inactivation of PME in orange (cv. Wakro) juice.

### 4.3.4 Effect of ACP treatment on *E. coli* inactivation

The initial log CFU/mL of *E. coli* was 7.44 ± 0.03. **Fig. 4.5** shows that the ACP treatment effectively inactivated the *E. coli* in orange (cv. Wakro) juice while extending the treatment time (0.5–3 min) under the same voltage. At 24 kV for 3 min, log CFU/mL for *E. coli* was achieved by 2.45 ± 0.21, indicating higher voltage resulted in faster inactivation of *E. coli* in orange (cv. Wakro) juice (**Fig. 4.5**). A 5-log cycle reduction was accomplished in just 3 min, probably due to the higher concentration of plasma reactive species, which effectively eliminated *E. coli* in the juice. At the voltage of 24 kV, treatment with only 1.5 min resulted in 4.49 ± 0.14 CFU/mL in activation of *E. coli*. Nonetheless, the 20 kV voltage required 3 min of treatment to achieve 4.43 ± 0.07 log CFU/mL. However, at 16 kV voltage, ACP treatment with 3 min showed 5.87 ± 0.02 log CFU/mL in juice. Therefore, the study revealed that ACP is voltage-dependent when inactivating *E. coli* in orange juice (cv. Wakeo). Other studies also demonstrated that the ACP could more efficiently inactivate *E. coli* in various food matrices (Liao et al., 2018; Sauza et al., 2023). The study's results also indicate that the *E. coli* is susceptible to ACP treatment since their total viable counts were considerably reduced within the range of treatment duration (0.5–3 min). The inactivation of *E. coli* by CP primarily disrupts the bacterial cell membrane (Nwabor et al., 2022). The reactive species like oxygen reactive species (ROS) and nitrogen reactive species (RNS) produced by CP in orange (cv. Wakro) juice may be responsible for the disruption of microbial cell walls, leading to inactivation or reduction of the survival population (Ikawa et al., 2010; Joshi et al., 2011). Numerous investigations have shown that the ROS and RNS obtained from CP could oxidize and attack the lipid bilayer of cell walls, resulting in a leakage of intercellular components and the eventual death of microbial cells (Liao et al., 2018; Joshi et al., 2011; Alkawareek et al., 2014).

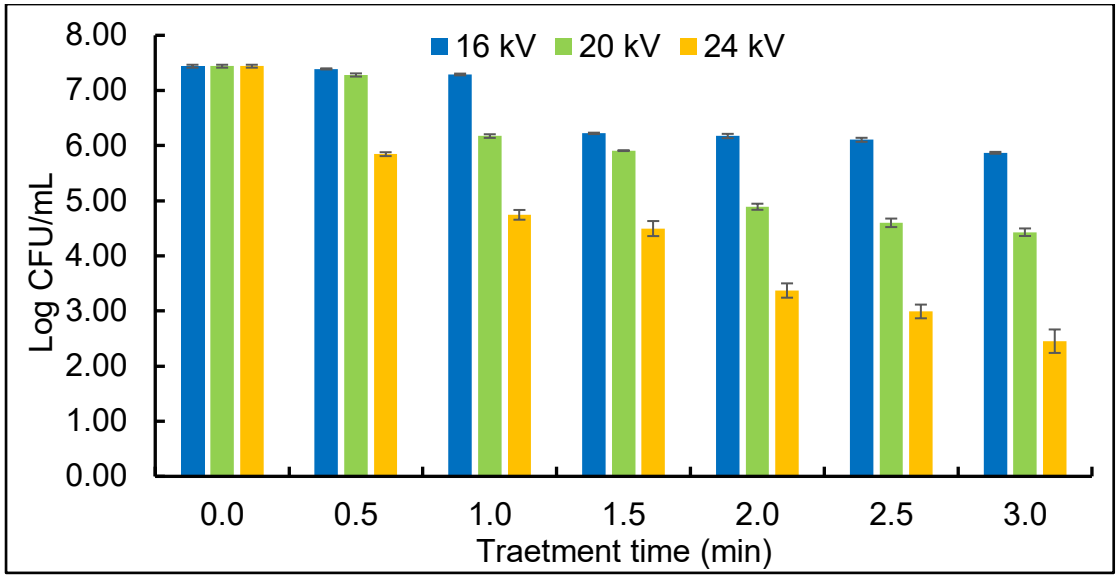


**Fig. 4.5** Survival population of microbe (*Escherichia coli*) in orange (cv. Wakro) juice after atmospheric cold plasma (ACP) treatment.

### 4.3.5 Inactivation kinetics modelling of *E. coli*

In the kinetic study, the log reduction of *E. coli* was plotted against the plasma treatment time to examine the kinetics behavior using different models. The kinetic profiles of the survival curves of tested microorganism (*E. coli*) were obtained from the fitted log-linear, Weibull, and Membre model (**Fig. 4.6**). The estimated model constant and goodness-of-fit parameters derived from fitted models with experimental data for the inactivation kinetics of *E. coli* are shown in **Table 4.3.**

**Table 4.3** Model constant parameters and goodness of fit for *E. coli*.

| **Model** | **Parameters** | ***E. coli*** | | |
|---|---|---|---|---|
| | | **16 kV** | **20 kV** | **24 kV** |
| log-linear | k ($min^{-1}$) | 1.2780 ± 0.43 | 2.5210 ± 0.43 | 4.2700 ± 0.89 |
| | $R^2$ | 0.8625 | 0.9558 | 0.9077 |
| | RMSE | 0.2581 | 0.2600 | 0.5303 |
| Weibull | B | 1.0760 ± 1.23 | 0.9746 ± 0.59 | 0.6247 ± 0.17 |
| | δ (min) | 0.8450 ± 1.04 | 0.3788 ± 0.42 | 0.0599 ± 0.06 |
| | $R^2$ | 0.8643 | 0.9561 | 0.9914 |
| | RMSE | 0.2808 | 0.2841 | 0.1775 |
| Membre | k ($min^{-1}$) | 0.3436 ± 0.09 | 0.5115 ± 0.10 | 0.6537 ± 0.17 |
| | $R^2$ | 0.8223 | 0.8287 | 0.4791 |
| | RMSE | 0.2933 | 0.5119 | 1.2600 |

#### 4.3.5.1 log-linear model

The estimated log-linear model constant (k) and goodness-of-fit parameters ($R^2$ and RMSE) for *E. coli* inactivation kinetics are presented in **Table 4.3**. The survival curve of the log-linear model fitting is shown in **Fig. 4.6a**. As observed in **Table 4.3**, the

inactivation rate constant (k) increased with increasing the voltage (16–24 kV), indicating ACP significantly affected the *E. coli* in orange (cv. Wakro) juice (**Table 4.3**). A lower value of k implies a slower inactivation rate. The $R^2$ value of the first-order model was comparatively lower than the Weibull model in all the cases of voltages, as shown in **Table 4.2**. However, the RMSE values at voltage 16 kV and 20 kV were obtained minimum compared to the Weibull model, indicating lower prediction error (**Table 4.2**). On the other hand, at 20 kV voltage, the $R^2$ value of the log-linear model was greater than that of the Weibull model, as observed in **Table 4.2**. With these consequences, it cannot be confirmed that the log-linear model has a good correlation.

#### 4.3.5.2 Weibull model

The Weibull model was successfully fitted to the experimental data after ACP treatment, as seen in **Fig. 4.6b. and Table 4.3**. The value of the shape factor, $\beta < 1$ at voltage 20 kV and 24 kV, exhibits that the inactivation curve has upward concavity or tailing, whereas $\beta > 1$ indicates downward concavity at voltage 16 kV. This upward concavity is formed mainly due to the fast inactivation of sensitive cells of the microbial population and the slow inactivation of resistant cells (Peleg, 2006; Feng et al., 2008). Esua et al. (2022) observed that tailing (upward concavity) with $\beta < 1$ during *E. coli* inactivation by the CP. Pokhrel et al. (2017) also observed downward concavity during *E. coli* inactivation in carrot juice was achieved by combined ultrasound and heat treatment. It was observed that the scale factor ($\delta$) decreased from 0.8450 to 0.0599 min (**Table 4.3**). Decreasing the $\delta$ values was also reported for the inactivation of *E. coli* with increasing the voltage during ACP treatment (Liao et al., 2018).

#### 4.3.5.3 Membre model

The convex shape of the fitting curve of the Membre model during *E. coli* inactivation by ACP is shown in **Fig. 4.6c.** In this model, k ($min^{-1}$) increased with the voltage, indicating *E. coli* was significantly inactivated by ACP, as seen in **Table 4.3.** Regarding the $R^2$ value ranging from 0.8223 to 0.479, the Membre model showed poorer data fit than the Weibull and log-linear model. This model produced higher RMSE than log-linear and Weibull, indicating that the prediction error was more distant from the observed value (**Table 4.3**).

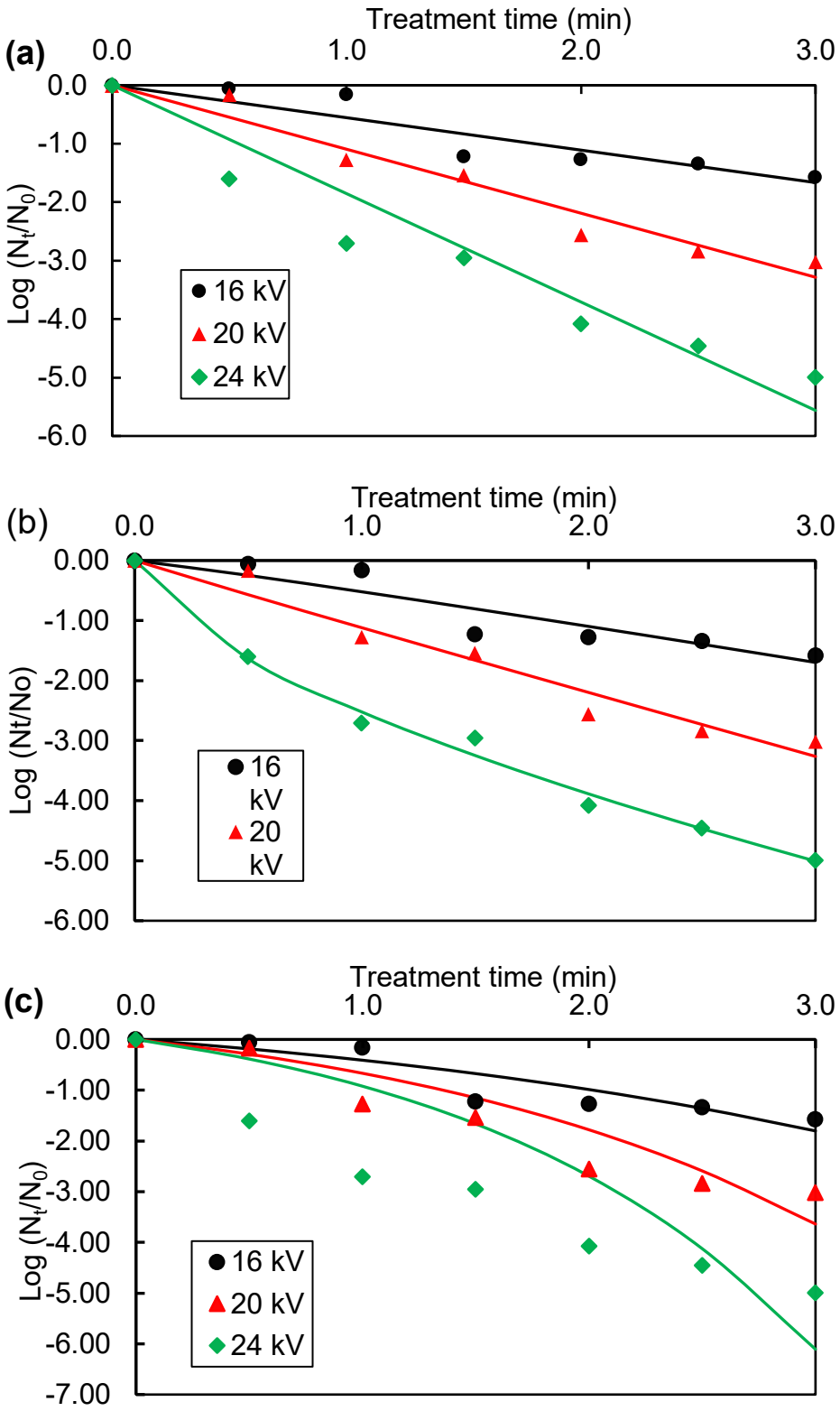


**Fig. 4.6** *E. coli* (MTCC 40) inactivation kinetics at different voltages (16–24 kV) (a) log-linear model, (b) Weibull model, and (c) Membre model. Different color marks (▲, ♦, ●) and lines (—, —, —) in the graphs indicated the experimental and predicted values of the log reduction (Log $N_t/N_0$).

### 4.3.6 Model validation and selection for *E. coli* inactivation

#### 4.3.6.1 Performance of the models and their validation

Apart from the standard statistics, the $A_f$ and $B_f$ were employed further to validate the models' performance (**Table 4.4**). If the $A_f$ and $B_f$ values show close to 1, the model predictions are accurate, and there is no over and under prediction (Jaiswal and Srivastava, 2024). At all conditions, the actual factor ($A_f$) for log-linear, Weibull, and Membre model of inactivation kinetics were in the range from 1.0054–1.0093, 1.0038–1.0000, and 1.0049–1.0388, respectively (**Table 4.4**). The $A_f$ values with all CP voltages exhibited close to 1, indicating minimal deviations between the predicted and experimental data. For pathogen inactivation models, Ross (1999) classified $B_f$ value as good in the range of 0.90–1.05, acceptable in the range of 0.70–0.90 or 1.06–1.15, and as unacceptable for values less than 0.70 or greater than 1.15. The $B_f$ values for the log-linear and Weibull models showed close to 1, whereas the Membre model with all CP voltage exhibited less than 1 (**Table 4.4**). $B_f$ values close to 1 indicate good agreement between observed and predicted values, whereas a $B_f$ smaller than 1 indicates under-prediction (Pokhrel et al., 2017). According to Ross (1999), the $B_f$ values of the log-linear and Weibull models are in the good range. The $B_f$ values of the Membre model with CP voltage 16 kV showed a good range (except 20 kV and 24 kV), as shown in **Table 4.4**. Comparing and assessing each model's overall performance was challenging with these $A_f$ and $B_f$ indices.

**Table 4.4** Model validation and selection for *E. coli.*

| **Model** | **Parameters** | ***E. coli*** | | |
|---|---|---|---|---|
| | | **16 kV** | **20 kV** | **24 kV** |
| Log-linear | $A_f$ | 1.0054 | 1.0015 | 1.0093 |
| | $B_f$ | 1.0054 | 1.0015 | 0.9908 |
| | AIC | -33.17 | -41.74 | -7.97 |
| | $\Delta_i$ | 1.00 | 0.00 | 101.99 |
| Weibull | $A_f$ | 1.0038 | 1.0020 | 1.0000 |
| | $B_f$ | 1.0268 | 1.0143 | 1.0000 |
| | AIC | -34.17 | -33.07 | -109.96 |
| | $\Delta_i$ | 0.00 | 8.67 | 0.00 |
| Membre | $A_f$ | 1.0049 | 1.0168 | 1.0388 |
| | $B_f$ | 0.9665 | 0.8900 | 0.7659 |
| | AIC | -33.01 | -6.48 | 12.52 |
| | $\Delta_i$ | 0.16 | 35.27 | 122.48 |

#### 4.3.6.2 Model selection by the Akaike information criterion and Akaike increment

The model's prediction error is assessed using the AIC, which also serves as a statistical tool to rank and choose the model that best fits the data (Kumar et al., 2024b). The previously discussed statistical matrices faced difficulty selecting the most suitable model among tested competing models. Therefore, AIC and $\Delta_i$ parameters were introduced as the alternatives to determine the best-fit model. The AIC and $\Delta_i$values of the tested models were summarized in **Table 4.4**. The model best matches experimental data, while the AIC ($\Delta_i$ = 0) values are relatively small (Panigrahi et al., 2021; Kumar et al., 2024a). The AIC and $\Delta_i$ values of the Membre model showed more than log-linear and Weibull models, as observed in **Table 4.4.** Thus, the criteria theory suggests that the Membre model does not match the observed data. Further, the log-liner and Weibull model were also compared using the values of AIC and $\Delta_i$. The AIC values of the log-linear model were observed more at a voltage of 24 kV and less at 20 kV, while at 16 kV, they showed the same as the Weibull model (**Table 4.4**). On the other hand, $\Delta_i$ values of the Weibull model were found to be zero at voltage 16 kV and 24 kV except for 20 kV ($\Delta_i$= 8.67). This indicates that the Weibull model with CP voltage 16 kV and 24 kV has significant support, while $\Delta_i$= 8.67 at 20 kV received less substantial support. According to the Akaike increment thumb rule, the Weibull model was established as the best-fit model for predicting the inactivation of *E. coli* in the ACP-treated juice for a specific data set. The Weibull model can also be considered the best-fit model.

### 4.4 Conclusion

The impact of ACP on PME and *E. coli* inactivation with kinetics modelling was investigated at different voltages (16–24 kV) as a function of time (0.5–3 min). The study revealed that the ACP parameters significantly affected the PME activity and *E. coli* in orange (cv. Wakro) juice. In the tested models, the inactivation rate constant, k, increases with the increase in voltage (16–24 kV), indicating that CP voltage significantly impacted the PME and *E. coli* inactivation in orange (cv. Wakro) juice. Higher voltage with extended treatment time showed a greater inactivation rate of PME and *E. coli*. This could be attributed to the large production of reactive species from CP, which leads to a faster inactivation rate. The $n^{th}$-order model showed the highest fitting accuracy for PME inactivation ($R^2 > 0.98$; RMSE < 0.012; $\Delta_i = 2$). On

the other hand, the Weibull model was best suited for *E. coli* inactivation kinetics ($R^2 > 0.85$; RMSE < 0.2841; $\Delta_i = 0$ (for 16 and 24 kV) and $\Delta_i = 8.67$ (for 20 kV)). The accuracy factor ($A_f$) and bias factor ($B_f$) for the respective models of PME and *E. coli* inactivation were close to the simulation line (closer to 1), suggesting the accuracy of these models in predicting. The study's results demonstrate the potential use of ACP treatment to maintain fruit juices' microbial safety and quality stability.

## Bibliography

Akaike, H. (1998). Information theory and an extension of the maximum likelihood principle. In *Selected Papers of Hirotugu Akaike* (pp. 199-213). Springer.

Alkawareek, M. Y., Gorman, S. P., Graham, W. G., & Gilmore, B. F. (2014). Potential cellular targets and antibacterial efficacy of atmospheric pressure non-thermal plasma. *International Journal of Antimicrobial Agents*, *43*(2), 154-160.

Andreou, V., Giannoglou, M., Xanthou, M. Z., Passaras, D., Kokkoris, G., Gogolides, E., & Katsaros, G. (2023). Inactivation of pectin methylesterase in fresh orange juice by cold atmospheric plasma technology: A kinetic study. *Innovative Food Science & Emerging Technologies*, *86*, 103361.

Arya, S. S., More, P. R., Das, T., Hilares, R. T., Pereira, B., Arantes, V., da Silva, S. S. & dos Santos, J. C. (2023). Effect of hydrodynamic cavitation processing on orange juice physicochemical and nutritional properties. *Journal of Agriculture and Food Research*, *14*, 100781.

Basak, S., & Ramaswamy, H. S. (1996). Ultra high pressure treatment of orange juice: a kinetic study on inactivation of pectin methyl esterase. *Food Research International*, *29*(7), 601-607.

Burnham, K. P., & Anderson, D. R. (2001). Kullback-Leibler information as a basis for strong inference in ecological studies. *Wildlife Research*, *28*(2), 111-119.

Chakraborty, S., Rao, P. S., & Mishra, H. N. (2015). Kinetic modeling of polyphenoloxidase and peroxidase inactivation in pineapple (*Ananas comosus* L.) puree during high-pressure and thermal treatments. *Innovative Food Science & Emerging Technologies*, *27*, 57-68.

Chutia, H., Kalita, D., Mahanta, C. L., Ojah, N., & Choudhury, A. J. (2019). Kinetics of inactivation of peroxidase and polyphenol oxidase in tender coconut water by dielectric barrier discharge plasma. *LWT-Food Science and Technology*, *101*, 625-629.

Dong, S., Fan, L., Ma, Y., Du, J., & Xiang, Q. (2021). Inactivation of polyphenol oxidase by dielectric barrier discharge (DBD) plasma: Kinetics and mechanisms. *LWT-Food Science and Technology*, *145*, 111322.

Esua, O. J., Sun, D. W., Ajani, C. K., Cheng, J. H., & Keener, K. M. (2022). Modelling of inactivation kinetics of *Escherichia coli* and *Listeria monocytogenes* on grass carp treated by combining ultrasound with plasma functionalized buffer. *Ultrasonics Sonochemistry*, *88*, 106086.

FDA, U.S. Food and Drug Administration. (2001). FDA Centre for Food Safety and Applied Nutrition, Bacteriological Analytical Manual.

Feng, H., Yang, W., & Hielscher, T. (2008). Power ultrasound. *Food Science and Technology International*, *14*(5), 433-436.

Hosseini, S. M., Rostami, S., Hosseinzadeh Samani, B., & Lorigooini, Z. (2020). The effect of atmospheric pressure cold plasma on the inactivation of Escherichia coli in sour cherry juice and its qualitative properties. *Food Science & Nutrition*, *8*(2), 870-883.

Ikawa, S., Kitano, K., & Hamaguchi, S. (2010). Effects of pH on bacterial inactivation in aqueous solutions due to low-temperature atmospheric pressure plasma application. *Plasma Processes and Polymers*, *7*(1), 33-42.

Jaiswal, M., & Srivastava, B. (2024). Evaluating the impact of pulsed light treatment on microbial and enzyme inactivation and quality attributes in fresh-cut watermelon. *Journal of Food Process Engineering*, *47*(5), e14626.

Joshi, S. G., Cooper, M., Yost, A., Paff, M., Ercan, U. K., Fridman, G., Friedman, G., Fridman, A., & Brooks, A. D. (2011). Nonthermal dielectric-barrier discharge plasma-induced inactivation involves oxidative DNA damage and membrane lipid peroxidation in *Escherichia coli*. *Antimicrobial Agents and Chemotherapy*, *55*(3), 1053-1062.

Kumar, A., & Srivastava, B. (2024). Inactivation of polyphenol oxidase and peroxidase in pineapple juice during continuous ohmic heating and modeling of inactivation kinetics during isothermal holding. *Journal of Food Process Engineering*, *47*(3), e14565.

Kumar, A., Kumar, M., Mahboob, M. R., & Srivastava, B. (2024). Influence of °Brix/Acid, and flow rate of pineapple juice and electric field strength on the performance of continuous ohmic heating system. *Journal of Food Science and Technology*, *61*(6), 1188-1200.

Kumar, S., Pipliya, S., & Srivastav, P. P. (2023). $n^{th}$ order kinetic modelling of peroxidase and polyphenol oxidase inactivation in kiwifruit juice during cold plasma and thermal treatment. *Innovative Food Science & Emerging Technologies*, *89*, 103475.

Kumar, S., Pipliya, S., Srivastav, P. P., & Srivastava, B. (2024a). Non-linear models for microbial inactivation kinetics in kiwifruit juice using cold plasma treatment: the combined impact of applied voltage, juice depth and treatment time. *Journal of Food Science and Technology*, 1–13.

Kumar, S., Pipliya, S., Srivastav, P. P., & Srivastava, B. (2024b). Modeling the inactivation kinetics of polyphenol oxidase and peroxidase during the cold plasma treatment of kiwifruit juice. *Journal of Food Process Engineering*, *47*(2), e14542.

Lacroix, N., Fliss, I., & Makhlouf, J. (2005). Inactivation of pectin methylesterase and stabilization of opalescence in orange juice by dynamic high pressure. *Food Research International*, *38*(5), 569-576.

Lee, T. H., Chua, L. S., Tan, E. T. T., Yeong, C., Lim, C. C., Ooi, S. Y., Aziz, R. B. A., Aziz, A. B., & Sarmidi, M. R. B. (2009). Kinetics of thermal inactivation of peroxidases and polyphenol oxidase in pineapple (*Ananas comosus*). *Food Science and Biotechnology*, *18*(3), 661-666.

Liao, X., Li, J., Muhammad, A. I., Suo, Y., Chen, S., Ye, X., Liu, D., & Ding, T. (2018). Application of a dielectric barrier discharge atmospheric cold plasma (Dbd-Acp) for *Eshcerichia coli* inactivation in apple juice. *Journal of Food Science*, *83*(2), 401-408.

Ludikhuyze, L., Ooms, V., Weemaes, C., & Hendrickx, M. (1999). Kinetic study of the irreversible thermal and pressure inactivation of myrosinase from broccoli (*Brassica oleracea* L. cv. Italica). *Journal of Agricultural and Food Chemistry*, *47*(5), 1794-1800.

Membré, J. M., Majchrzak, V., & Jolly, I. (1997). Effects of temperature, pH, glucose, and citric acid on the inactivation of Salmonella typhimurium in reduced calorie mayonnaise. *Journal of Food Protection*, *60*(12), 1497-1501.

Mošovská, S., Medvecká, V., Valík, Ľ., Mikulajová, A., & Zahoranová, A. (2023). Modelling of inactivation kinetics of *Escherichia coli, Salmonella Enteritidis* and *Bacillus subtilis* treated with a multi-hollow surface dielectric barrier discharge plasma. *Scientific Reports*, *13*(1), 12058.

Nwabor, O. F., Onyeaka, H., Miri, T., Obileke, K., Anumudu, C., & Hart, A. (2022). A cold plasma technology for ensuring the microbiological safety and quality of foods. *Food Engineering Reviews*, *14*(4), 535-554.

Panigrahi, C., Mishra, H. N., & De, S. (2021). Modelling the inactivation kinetics of *Leuconostoc mesenteroides, Saccharomyces cerevisiae* and total coliforms during ozone treatment of sugarcane juice. *LWT-Food Science and Technology*, *144*, 111218.

Pankaj, S. K., Misra, N. N., & Cullen, P. J. (2013). Kinetics of tomato peroxidase inactivation by atmospheric pressure cold plasma based on dielectric barrier discharge. *Innovative Food Science & Emerging Technologies*, *19*, 153-157.

Pankaj, S. K., Wan, Z., & Keener, K. M. (2018). Effects of cold plasma on food quality: A review. *Foods*, *7* (1), 4.

Peleg, M. (2006). *Advanced Quantitative Microbiology for Foods and Biosystems: Models for Predicting Growth and Inactivation*. CRC Press.

Pipliya, S., Kumar, S., & Srivastav, P. P. (2022). Inactivation kinetics of polyphenol oxidase and peroxidase in pineapple juice by dielectric barrier discharge plasma technology. *Innovative Food Science and Emerging Technologies*, *80*, 103081.

Pokhrel, P. R., Bermúdez-Aguirre, D., Martínez-Flores, H. E., Garnica-Romo, M. G., Sablani, S., Tang, J., & Barbosa-Cánovas, G. V. (2017). Combined effect of ultrasound and mild temperatures on the inactivation of *E. coli* in fresh carrot juice and changes on its physicochemical characteristics. *Journal of Food Science*, *82*(10), 2343-2350.

Rizvi, A. F., & Tong, C. H. (1997). Fractional conversion for determining texture degradation kinetics of vegetables. *Journal of Food Science*, *62*(1), 1-7.

Ross, T. (1996). Indices for performance evaluation of predictive models in food microbiology. *Journal of Applied Bacteriology*, *81*(5), 501-508.

Ross, T. (1999). Predictive food microbiology models in the meat industry. In *Meat and Livestock Australia* (pp. 196). Australia.

Santos Jr, L. C. O., Cubas, A. L. V., Moecke, E. H. S., Ribeiro, D. H. B., & Amante, E. R. (2018). Use of cold plasma to inactivate Escherichia coli and physicochemical evaluation in pumpkin puree. *Journal of Food Protection*, *81*(11), 1897-1905.

Saxena, J., Makroo, H. A., Bhattacharya, S., & Srivastava, B. 92017). Kinetics of the inactivation of polyphenol oxidase and formation of reducing sugars in sugarcane juice during Ohmic and conventional heating. *Journal of Food Process Engineering*, *41*(3), e12671.

Serment-Moreno, V., Fuentes, C., Barbosa-Cánovas, G., Torres, J. A., & Welti-Chanes, J. (2015). Evaluation of high pressure processing kinetic models for microbial inactivation using standard statistical tools and information theory criteria, and the development of generic time-pressure functions for process design. *Food and Bioprocess Technology*, *8*, 1244-1257.

Shalini, G. R., Shivhare, U. S., & Basu, S. (2008). Thermal inactivation kinetics of peroxidase in mint leaves. *Journal of Food Engineering*, *85*(1), 147-153.

Souza, D. V. S., Melo, M. F., Ambrósio, M. M. Q., Alves, C., Melo, N. J. A., Costa, L. L., & Morais, P. L. D. (2023). Effect of plasma and heat treatments on orange juice quality. *Brazilian Journal of Biology*, *83*, e272709.

Van Impe, J., Smet, C., Tiwari, B., Greiner, R., Ojha, S., Stulić, V., Vukušić, T., & Režek Jambrak, A. (2018). State of the art of nonthermal and thermal processing for inactivation of microorganisms. *Journal of Applied Microbiology*, *125*(1), 16-35.

Vega, S., Saucedo, D., Rodrigo, D., Pina, C., Armero, C., & Martínez, A. (2016). Modeling the isothermal inactivation curves of *Listeria innocua* CECT 910 in a vegetable beverage under low-temperature treatments and different pH levels. *Food Science and Technology International*, *22*(6), 525-535.

Weemaes, C. A., Ludikhuyze, L. R., Van den Broeck, I., & Hendrickx, M. E. (1998). Effect of pH on pressure and thermal inactivation of avocado polyphenol

oxidase: a kinetic study. *Journal of Agricultural and Food Chemistry*, *46*(7), 2785-2792.

Xu, L., Garner, A. L., Tao, B., & Keener, K. M. (2017). Microbial inactivation and quality changes in orange juice treated by high voltage atmospheric cold plasma. *Food and Bioprocess Technology*, *10*, 1778-1791.